

A New Strategy toward “Simple” Water-Soluble AIE Probes for Hypoxia Detection

Changhuo Xu, Hang Zou, Zheng Zhao, Pengfei Zhang, Ryan T. K. Kwok, Jacky W. Y. Lam, Herman H. Y. Sung, Ian D. Williams, and Ben Zhong Tang*

Hypoxia-responsive fluorescent probes have emerged as a novel scaffold for tumor diagnosis. However, dilemma often exists between simple synthesis and high water solubility in traditional probes. Owing to the intrinsic property of N-oxides, herein, a new strategy is proposed to design and synthesize probes for in vitro hypoxia imaging. Equipped with tetraphenylethene (TPE), the N-oxides exhibit aggregation-induced emission characteristics and emit no light in aqueous solutions. Interestingly, the N-oxides can be reduced by ferrous ions in different rates. The aggregation of the resulting hydrophobic TPE residues restricts the intramolecular motions of the molecules, which “turns-on” their fluorescence. The N–O covalent bond of one molecule can be specifically cleaved by cellular reductase overexpressed under hypoxic conditions, and thus turn-on hypoxia imaging in vitro is achieved. The new strategy to design hypoxia imaging probes is extremely valuable and has great potential for application in tumor diagnosis.

sensitivity and precision can help surgeons visualize tiny disseminated tumors and launch preventive and therapeutic measures. Hypoxia, or oxygen depletion, arises in solid tumors as a consequence of the imbalance between aberrant blood vessel formation and increased oxygen demands for tumor cell proliferation.^[1] Unlike adequate oxygenation of normal tissues, which is physiologically compensated through a regulable blood flow,^[2] tumors tend to develop intense hypoxia even with a diameter of 1–2 mm.^[3] Utilizing this unique characteristic of tumors, imaging hypoxic areas can achieve precise detection of early tumor formation and early spread of metastatic tumor cells.

Positron emission tomography and single photon emission computed tomography

have been widely exploited to image hypoxic areas via radiotracers conjugated with a hypoxia-sensitive trigger, such as ¹⁸F-fluoromisonidazole and ⁶⁴Cu-diacetyl-bis (N₄-methylthiosemicarbazone).^[4] However, their working mechanism is based on the enhancement of tracer retention, and fails to provide an off-on detection signal. In addition, the accumulation of these probes at the tumor site requires a very low oxygen level, which may hinder precise detection.^[5] Because of these limitations, it is thus highly desirable to develop hypoxia imaging modalities with high sensitivity and excellent specificity. Fluorescence imaging has become one of the most powerful real-time imaging modalities for inspecting biological processes in vitro and in vivo. Thus, developing hypoxia-responsive fluorescent probes is regarded as a promising strategy to accurately visualize tumors with oxygen deficiency. According to the reported literature, fluorescence-based hypoxia probes generally comprise one chromophore and one hypoxia-sensitive moiety (Scheme S1, Supporting Information).^[6] Once the probes are internalized by cells, the overexpressed reductases under hypoxic conditions will cleave the hypoxia-sensitive moieties to recover their intrinsic fluorescence. Although the existing fluorescent probes show an excellent analytical performance of hypoxia detection, there are still some bottlenecks to limit their further development, such as complexity in synthesis, poor water solubility, toxicity of the formative metabolite, and poor biocompatibility.^[7] Overall, exploring a water-soluble hypoxia-sensing probe through easy and smart chemistry is in high demand for tumor diagnosis.

Aggregation-induced emission luminogens (AIEgens) are propeller-shaped molecules emitting strong fluorescence in

1. Introduction

Tumor diagnosis in the early stage is vitally important as it enables successful cancer treatment and high survival rate of patients. Noninvasive imaging of early tumors with high

C. Xu, H. Zou, Dr. Z. Zhao, Dr. P. Zhang, Dr. R. T. K. Kwok, Dr. J. W. Y. Lam, Dr. H. H. Y. Sung, Prof. I. D. Williams, Prof. B. Z. Tang
Department of Chemistry
The Hong Kong Branch of Chinese National Engineering Research Center for Tissue Restoration and Reconstruction
Institute of Molecular Functional Materials
Division of Life Science and State Key Laboratory of Molecular Neuroscience
and Institute for Advanced Study
The Hong Kong University of Science and Technology
Clear Water Bay, Kowloon, Hong Kong 999077, China
E-mail: tangbenz@ust.hk

H. Zou
Department of Laboratory Medicine
Nanfang Hospital
Southern Medical University/The First School of Clinical Medicine
Southern Medical University
Guangzhou 510515, China

Prof. B. Z. Tang
Center for Aggregation-Induced Emission
SCUT-HKUST Joint Research Institute
State Key Laboratory of Luminescent Materials and Devices
South China University of Technology
Guangzhou 510640, China

 The ORCID identification number(s) for the author(s) of this article can be found under <https://doi.org/10.1002/adfm.201903278>.

DOI: 10.1002/adfm.201903278

the aggregate or solid state but low fluorescence in the solution state.^[8] Based on a wealth of experimental and theoretical studies, the restriction of intramolecular motion (RIM) has been proposed as the main mechanistic picture of the aggregation-induced emission (AIE) effect.^[9] Due to the intriguing photophysical properties of AIEgens, many researchers have been working on the development of fluorescent probes with AIE features to realize the imaging of specific substrates in a fluorescence “turn-on” manner.^[10] A typical design strategy of AIEgen-based probes is to endow the AIE-active molecules with water solubility and emission turn-off property in the solution state. Additional specific moieties are incorporated that can physically or chemically interact with substrates to form polymers, crosslinked networks, or aggregates to trigger a turn-on fluorescence signal. For example, tetrazole-tagged AIE luminogen, namely TPE-4TA, can efficiently coordinate with Ag⁺ ions in solution to form fluorescent coordinated polymers.^[11]

Inspired by the hypoxia-responsive property of a prodrug, called AQ4N,^[12] we synthesized a tetraphenylethene (TPE) derivative with N-oxide groups (TPE-2OM N-oxide), but unfortunately the molecule was not water soluble (Figure S1, Supporting Information). Alternatively, we herein presented the facile synthesis of three new molecules, namely TPE-2M N-oxide, TPE-2E N-oxide, and TPE-2M2F N-oxide, with good water solubility for in vitro hypoxia imaging in a fluorescent turn-on manner. The zwitterionic N-oxide groups not only enabled the AIEgens to dissolve in water but also endowed them with sensitivity to reducing species. The sensitivity to reducing agents was tunable through the introduction of electron-withdrawing groups into TPE-2M2F N-oxide or hydrophobic alkyl chains into TPE-2E N-oxide. The neutral nature of the N-oxides also made them inert to positively or negatively charged interferences in living cells. Because of the active intramolecular motion, the water-soluble TPE-containing N-oxides were nonemissive. Under hypoxic conditions, the overexpressed reductase catalyzed the reduction of the N-oxides to the corresponding amines via irreversible two-electron reduction.^[13] Since the amine forms of the new molecules were insoluble in aqueous media, their aggregates emitted strong photoluminescence (Scheme 1).

2. Results and Discussion

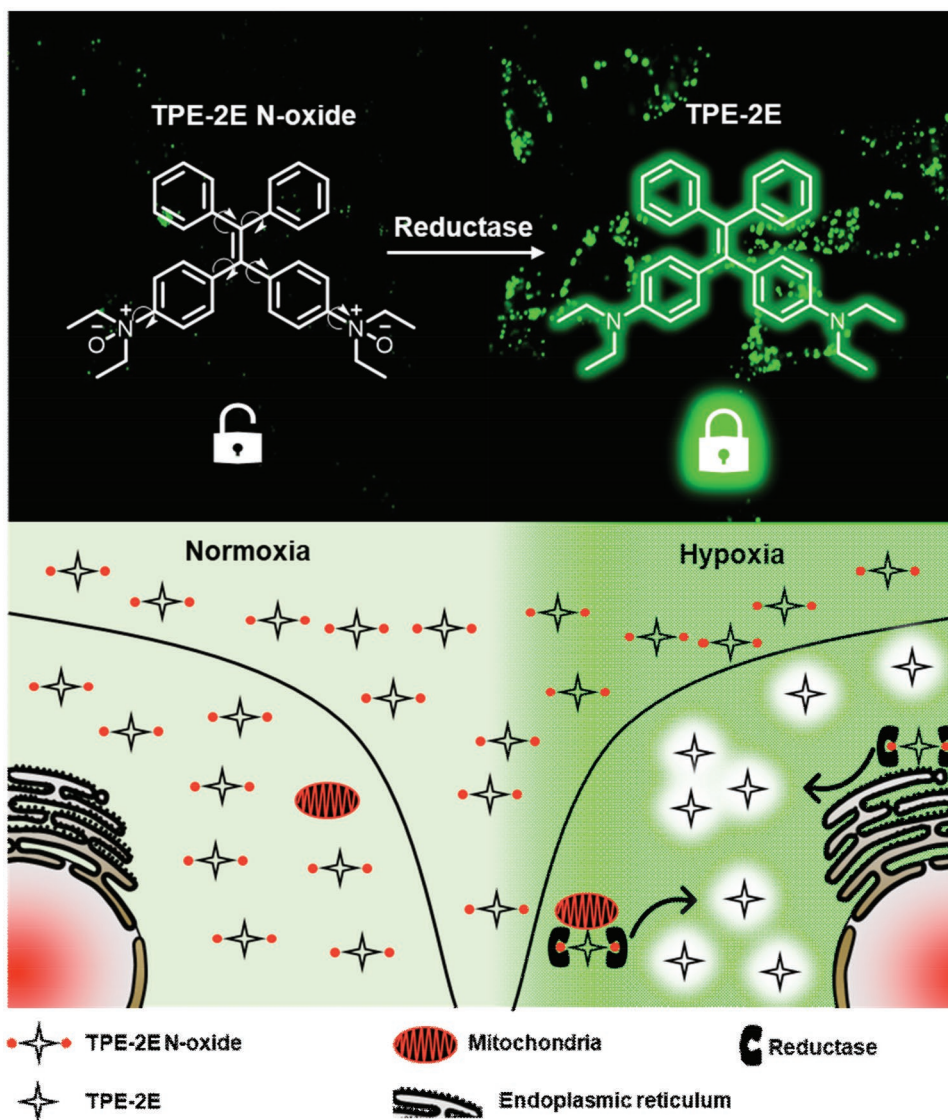
2.1. Design and Synthesis of the N-Oxides

The synthetic route and chemical structures of TPE-2M N-oxide, TPE-2E N-oxide, and TPE-2M2F N-oxide are shown in Figure 1A. Taking TPE-2M N-oxide as an example, it was synthesized in a total yield of 30% via McMurry cross-coupling reaction of 4,4'-bis(dimethylamino)-benzophenone and benzophenone followed by subsequent oxidation of the obtained TPE-2M. The synthetic details can be found in the “Experimental Section.” Figure 1B compared the ¹H NMR spectra of TPE-2M and TPE-2M N-oxide. The resonance peaks of c and d, respectively, shifted to c' and d' upon the oxidation of the dimethylamine group. A small downfield shift of water resonance peak was also observed, probably due to the formation of N-oxide hydrates. The structure of TPE-2M N-oxide was further confirmed by X-ray single-crystal analysis (Figure 1C;

Table S1, Supporting Information). The single-crystal structure of TPE-2M N-oxide showed the formation of intermolecular hydrogen bonds between water molecules and the N-oxide groups. It unraveled that N-oxide hydrates did exist and their hydrophilic nature was explained. All the precursors and final products were fully characterized by NMR spectroscopies with satisfactory results (Figures S2–S7, Supporting Information). The high-resolution mass spectroscopies of TPE-2M N-oxide, TPE-2E N-oxide, and TPE-2M2F N-oxide displayed *m/z* peaks corresponded to their exact molecular mass minus the mass of two oxygen atoms (Figures S8–S10, Supporting Information). TPE-2M N-oxide, TPE-2E N-oxide, and TPE-2M2F N-oxide are completely soluble in CHCl₃, dichloromethane (DCM), MeOH, dimethyl sulfoxide, and H₂O, but poorly soluble in hexane and ethyl acetate. The aqueous solutions of the N-oxides are exceptionally stable even when incubated at 70 °C for 24 h (Figure S11, Supporting Information).

2.2. Photophysical Properties of the N-Oxides

The photophysical properties of TPE-2M N-oxide, TPE-2E N-oxide, and TPE-2M2F N-oxide were characterized by UV–vis and photoluminescence (PL) spectroscopies (Figure 2). All the N-oxides were nonemissive in DCM. The PL of TPE-2M N-oxide and TPE-2M2F N-oxide was gradually intensified and blueshifted upon addition of hexane. At a hexane fraction (*f_H*) of 99%, the PL spectra blueshifted by 30–40 nm. This phenomenon could be deciphered by twisted intramolecular charge transfer mechanism (TICT).^[14] Considering that TPE-2M N-oxide and TPE-2M2F N-oxide possessed typical D–π–A structures, they adopted a twisted molecular conformation to reach an equilibrium with the surrounding polar dichloromethane molecules (TICT state). With increasing hexane fraction, the polarity of the DCM/hexane mixture decreased, and the more coplanar molecular conformation of TPE-2M N-oxide and TPE-2M2F N-oxide was stabilized. Thus, their PL spectra were dominated by the blueshifted emission of their locally excited state. The PL intensity of TPE-2M2F N-oxide reached the highest point at a hexane fraction of 90% but became lower at 99%. Based on the previous publications, a possible explanation was provided.^[15] In a mixture with a “low” hexane fraction of 90%, molecules of TPE-2M2F N-oxide might steadily cluster together to form ordered nanocrystalline particles. On the other hand, the molecules might form random agglomerates in a mixture with a very high hexane fraction of 99%. The different packing modes would lead to different fluorescence behaviors. The rigid structure of TPE-2M2F N-oxide in the crystalline state restricted the molecular motion in a greater extent to intensify the PL. In contrast, the random agglomerates devoted a certain space for active molecular motion to decrease the PL. Different from TPE-2M N-oxide and TPE-2M2F N-oxide, TPE-2E N-oxide only emitted strong PL in DCM/hexane mixture with an *f_H* of 99% (Figure 2B). This indicated TPE-2E N-oxide was more hydrophobic than TPE-2M N-oxide and TPE-2M2F N-oxide. The emission enhancement upon addition of a poor solvent into their well-solubilized solvent suggested that TPE-2M N-oxide, TPE-2E N-oxide, and TPE-2M2F N-oxide were all AIE-active (Figure 2D). Due to the RIM mechanism, it is legitimately



Scheme 1. Schematic illustration of hypoxia detection based on the hydrophilic to hydrophobic transition of TPE-2E N-oxide to TPE-2E catalyzed by intracellular reductases.

believed that the TPE-based N-oxides are nonemissive in other good solvents such as methanol and water. The UV spectra of the N-oxides in DCM were almost identical, showing an absorption peak at around 310 nm (Figure 2E). The photophysical properties of the precursors (TPE-2M, TPE-2E, and TPE-2M2F) were also investigated. They showed an absorption peak at about 360 nm and emitted a strong fluorescence at around 520 nm in tetrahydrofuran (THF)/water mixtures (Figure S12, Supporting Information). All the photophysical data were summarized in **Table 1**, including the quantum yields (QYs) of all compounds in solutions and solid films. Among TPE-2M, TPE-2E, and TPE-2M2F, TPE-2E showed the highest QY. To answer this question, we measured their PL spectra in solid films. As given in Figure S13A (Supporting Information), only TPE-2E showed bluer emission in solid film by 40 nm than its aqueous suspension at 99% water fraction. TPE-2E was found to be a crystallization-induced emission luminogen.^[16] The emission

maximum of TPE-2E in the crystalline state located at 480 nm. This implied that the solid film of TPE-2E was partially crystallized. The rigidification of the molecular structure of TPE-2E in the crystalline state hampered the aromatic rings from undergoing conformational changes caused by such movements as intramolecular rotations to enhance emission efficiency. TPE-2M2F N-oxide showed the lowest QY within three N-oxides. Through an internal comparison of their PL spectra in solid films, as shown in Figure S13B (Supporting Information), a shoulder peak highlighted by dash dot line in the emission spectrum of TPE-2M2F N-oxide was identified at 510 nm. It indicated that there were some sort of strong intermolecular interactions in the TPE-2M2F N-oxide film. These interactions could allow the loss of exciton energy through the nonradiative decay channel to decrease the fluorescence efficiency. The significant difference between the quantum yield of the solution and solid state also proved that these TPE derivatives and their

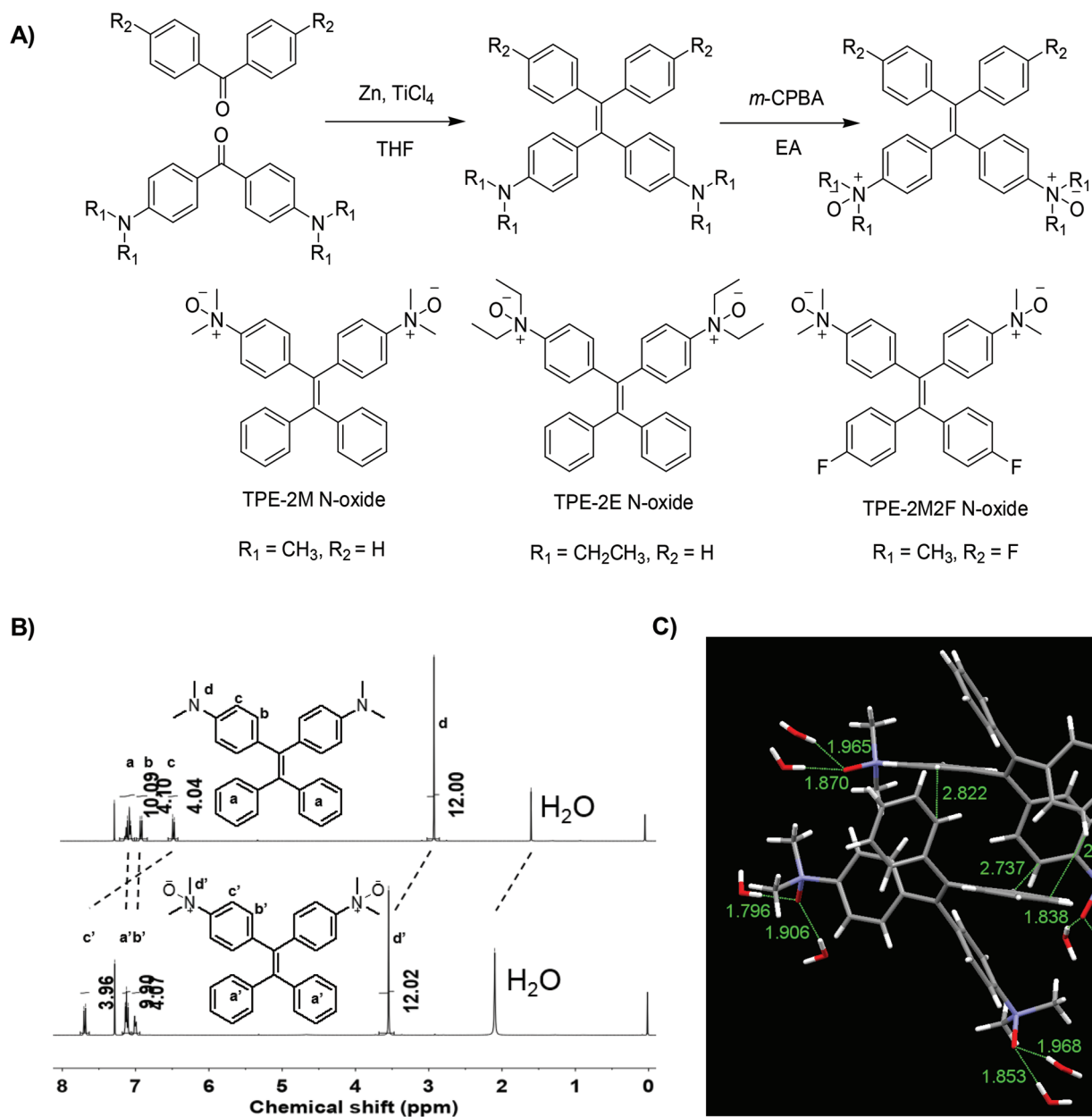


Figure 1. A) The synthetic route of N-oxides. B) ^1H NMR spectra of (top) TPE-2M and (bottom) TPE-2M N-oxide. C) Single-crystal structure of TPE-2M N-oxide.

corresponding N-oxides were AIE-active. The photos of TPE-2E and TPE-2E N-oxides in the solid state taken under daylight and UV light were shown in Figure 2F. Apparently, the absorption and PL spectra of the N-oxides were blueshifted from those of their amino counterparts, which could be ascribed to the change of the substituent property from electron donating (amino) to electron withdrawing (N-oxide).

2.3. Fluorescence Response to Ferrous Ions

Patterson et al. stated that N-oxides could undergo two-electron reduction via cytochrome P450 with a heme-iron center

as an active site (Scheme S2, Supporting Information).^[17] It thus encourages us to examine the fluorescence response of the present molecules to ferrous ions.^[18] We studied their PL in the presence of $(\text{NH}_4)_2\text{Fe}(\text{SO}_4)_2$. As shown in Figure 3A and Figure S14A (Supporting Information), the PL of TPE-2M and TPE-2M2F N-oxides at 520 nm increased remarkably by prolonging the incubation time with Fe^{2+} to 30 min at room temperature. The enhancement of the emission at 520 nm unveiled that the N-oxides were reduced to the corresponding TPE-2M and TPE-2M2F. As TPE-2M and TPE-2M2F were insoluble in water, emissive aggregates were formed. Moreover, TPE-2M2F N-oxide displayed a faster reduction rate by Fe^{2+} . In terms of the reported literatures, it was deduced that the

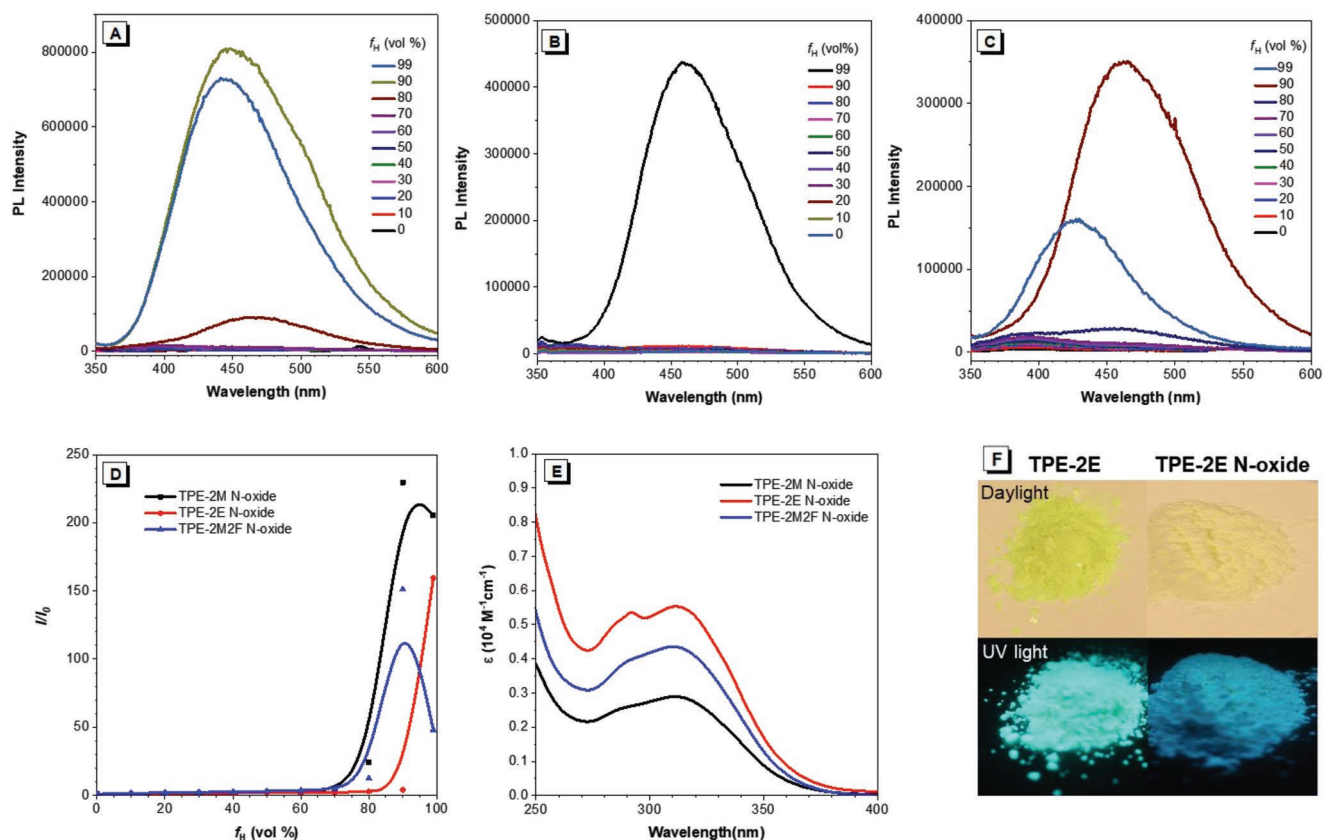


Figure 2. A–C) PL spectra of A) TPE-2M N-oxide, B) TPE-2E N-oxide, and C) TPE-2M2F N-oxide in DCM/hexane mixtures with different hexane fractions (f_H). D) Plot of relative peak intensity (I/I_0) versus f_H . Concentration: 10×10^{-6} M; excitation wavelength: 330 nm. E) Absorption spectra of TPE-2M N-oxide, TPE-2E N-oxide, and TPE-2M2F N-oxide in DCM. Concentration: 100×10^{-6} M. F) Photos of TPE-2E and TPE-2E N-oxide in the solid state taken under daylight (top) and UV light (bottom).

electron-withdrawing nature of the fluorine atoms caused an increase of the reduction potential to allow TPE-2M2F N-oxide to obtain electrons from Fe^{2+} more easily.^[19] However, TPE-2E N-oxide showed only a negligible response to Fe^{2+} under the same incubation condition (Figure S14B, Supporting Information). When the Fe^{2+} concentration was elevated to 1×10^{-3} M, conversion to TPE-2E occurred to give off fluorescence signal (Figure 3C; Figure S14C, Supporting Information). Thus, it could be speculated that the steric effect correlated with the reduction of the N-oxides by Fe^{2+} . As TPE-2E N-oxide was more hydrophobic than the other two N-oxides, it was reduced by

Fe^{2+} in a slower rate (Figure 3B). The reduction rates of TPE-based N-oxides were also inspected by the colorimetric sensing of Fe^{3+} , which was generated along with the reduction of the N-oxides. 3,3',5,5'-Tetramethylbenzidine (TMB) is one of the commonly used peroxidase substrates. It was reported that TMB could be directly oxidized by Fe^{3+} to produce a blue solution with absorption maximum at 652 nm.^[20] Thus, TMB could be used for colorimetric sensing of Fe^{3+} (Figure 3D). Therefore, the absorbance change of TPE-2M N-oxide, TPE-2E N-oxide, and TPE-2M2F N-oxide incubated with $(\text{NH}_4)_2\text{Fe}(\text{SO}_4)_2$ and TMB was characterized by UV-vis spectroscopy. As shown in

Table 1. Photophysical properties of TPE derivatives and their corresponding N-oxides.

Compounds	$\lambda_{\text{abs}}^{\text{a)}$ [nm]	$\lambda_{\text{em}}^{\text{b)}$ [nm]	$\lambda_{\text{em}}^{\text{c)}$ [nm]	QY ^{a)} [%]	QY ^{c)} [%]	Compound	$\lambda_{\text{abs}}^{\text{d)}$ [nm]	$\lambda_{\text{em}}^{\text{e)}$ [nm]	$\lambda_{\text{em}}^{\text{c)}$ [nm]	QY ^{f)} [%]	QY ^{c)} [%]
TPE-2M	362	519	516	0.6	8.3	TPE-2M N-oxide	312	444	448	0.6	17.4
TPE-2E	365	520	480	0.7	23.7	TPE-2E N-oxide	313	460	460	0.7	25.7
TPE-2M2F	360	515	509	0.7	17.2	TPE-2M2F N-oxide	312	427	442	0.5	6.1

^{a)} Measured in THF solution; ^{b)} Measured in THF/water mixtures with 99% fraction of water; ^{c)} Measured in solid film; ^{d)} Measured in DCM solution; ^{e)} Measured in DCM/hexane mixtures with 99% hexane fraction; ^{f)} Measured in water solution.

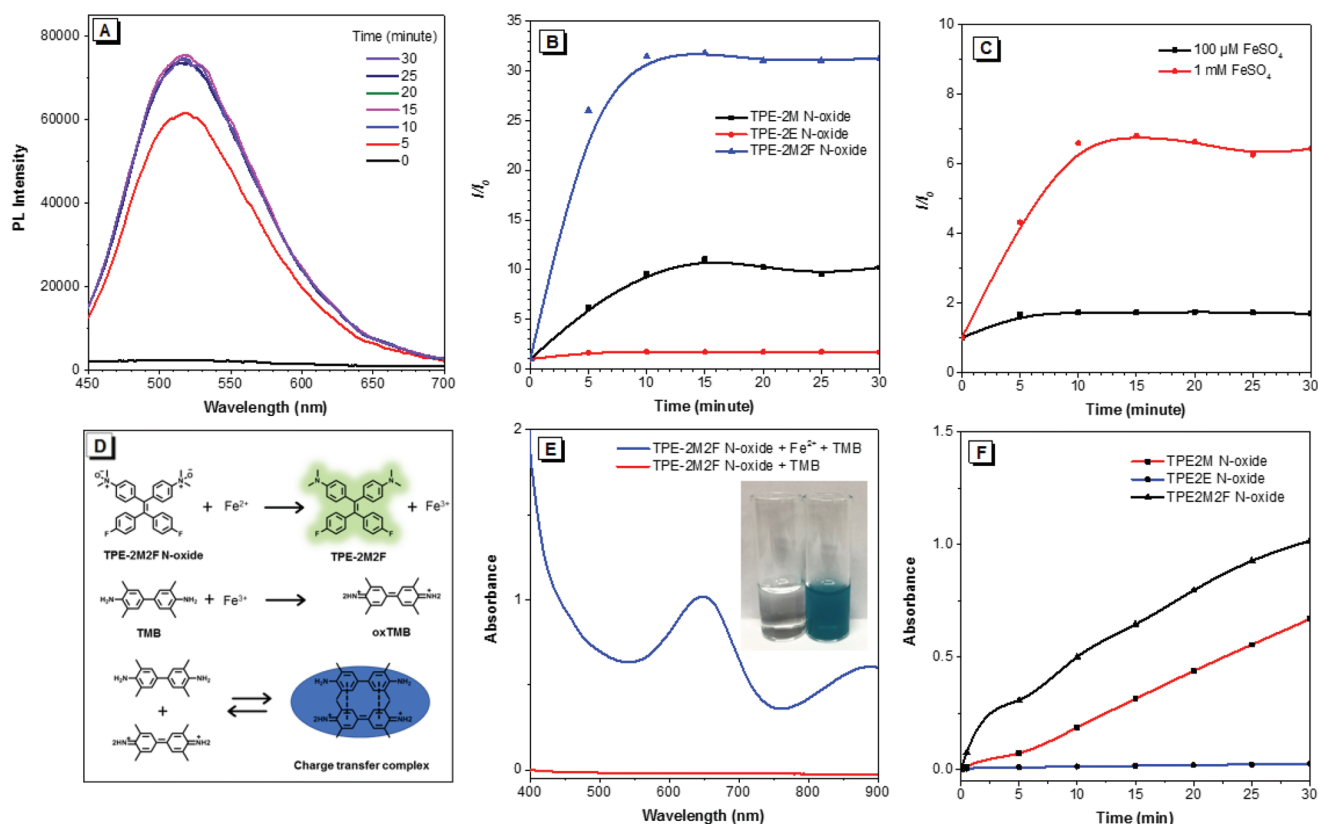


Figure 3. A) PL of TPE-2M2F N-oxide with time upon addition of 100×10^{-6} M of $(\text{NH}_4)_2\text{Fe}(\text{SO}_4)_2$. B) The kinetics of fluorescence change of TPE-2M N-oxide, TPE-2E N-oxide and TPE-2M2F N-oxide. C) The kinetics of fluorescence change of TPE-2E N-oxide in the presence of 100×10^{-6} M or 1×10^{-3} M $(\text{NH}_4)_2\text{Fe}(\text{SO}_4)_2$. All the data were obtained with a 10×10^{-6} M probe in 50×10^{-3} M 4-(2-hydroxyethyl)-1-piperazineethanesulfonic acid (HEPES) buffer (pH = 7.4). Excitation wavelength: 380 nm. D) Schematic representation of N-oxide reduction and TMB oxidation process. E) Absorbance change of 200×10^{-6} M TPE-2M2F N-oxide after incubated with 2×10^{-3} M $(\text{NH}_4)_2\text{Fe}(\text{SO}_4)_2$ and 200×10^{-6} M TMB or 200×10^{-6} M TMB only for 1 h. F) The kinetics of time-dependent absorbance change at 652 nm of TPE-2M N-oxide, TPE-2E N-oxide, and TPE-2M2F N-oxide incubated with 2×10^{-3} M $(\text{NH}_4)_2\text{Fe}(\text{SO}_4)_2$ and 200×10^{-6} M TMB at room temperature. All the experiments were performed in 50×10^{-3} M HEPES buffer (pH = 7.4) with 200×10^{-6} M of probe at room temperature.

Figure 3E, TMB hardly underwent oxidation at the presence of TPE-2M2F N-oxide only, whereas the solution turned blue when TMB was incubated with TPE-2M2F N-oxide and Fe^{2+} , as under circumstance TMB was oxidized to oxTMB. The oxidation rate of TMB to different N-oxides was investigated (Figure S15, Supporting Information). The rate of Fe^{3+} generation by the reaction of TPE-2M N-oxide and Fe^{2+} was modest. However, almost no Fe^{3+} was produced by the reaction of TPE-2E N-oxide and Fe^{2+} as the solution remained transparent. Due to the electron-withdrawing property of the fluorine substituents, Fe^{3+} was produced at the fastest rate when TPE-2M2F N-oxide reacted with Fe^{2+} . The kinetics of absorbance change in Figure 3F were fully consistent with the results from the previous fluorescence assay. It unveiled that the reduction rate of the N-oxide could be precisely regulated by different substituent groups.

To certify that the N-oxides were successfully reduced to the corresponding aniline by Fe^{2+} , we conducted the reduction experiment using TPE-2E N-oxide as the substrate. As shown in Figure 4A, the transparent solution containing 2×10^{-3} M of TPE-2E N-oxide became turbid with yellow precipitates upon the addition of $(\text{NH}_4)_2\text{Fe}(\text{SO}_4)_2$, which was validated by the size distribution measurement in Figure 4B. We analyzed the

extracts on the thin-layer chromatography plate and found that TPE-2E was the most abundant extract as predicted. ^1H NMR spectrum of the extracts was shown in Figure S16 (Supporting Information). Taking ^1H NMR spectrum of TPE-2E as reference, the corresponding resonance peaks of TPE-2E in the ^1H NMR spectrum of the extracts were clearly observed. The remaining resonance peaks were assigned to unreacted TPE-2E N-oxide or partially reduced TPE-2E N-oxide. This suggested that TPE-2E N-oxide did convert to TPE-2E in the presence of reducing agent, while emitting strong green fluorescence (Figure 4C). We further examined the selectivity of the N-oxides to other metal ions. As shown in Figure S17 (Supporting Information), none of these ions could turn on the fluorescence of the N-oxides except ferrous ions. The N-oxides could potentially interact with human serum albumin (HSA) by insertion into its hydrophobic pocket to trigger blue emission and also have the possibility to react with the thiols of HSA to induce green emission. Based on these two concerns, the PL measurement using two excitation sources (330 and 380 nm) was conducted to examine their physical and chemical interactions with proteins. It was proved that all the N-oxides showed no fluorescence response when incubated with HSA (Figure S18A,B, Supporting Information).

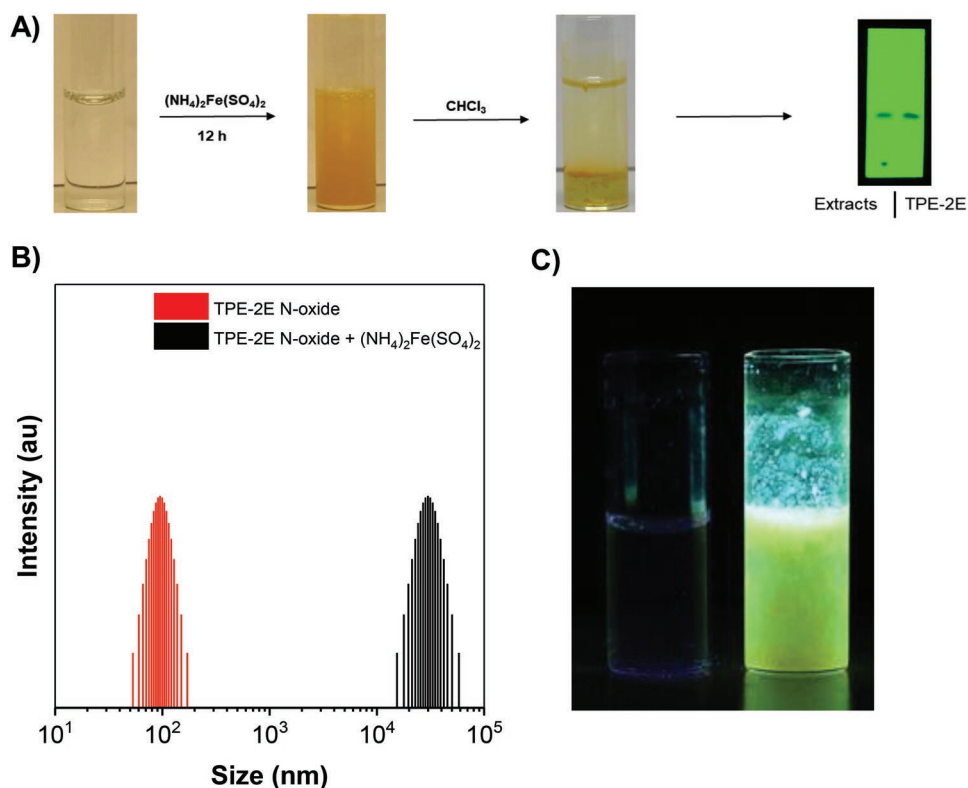


Figure 4. A) The conversion of TPE-2E N-oxide to TPE-2E in deionized (DI) water by addition of 20×10^{-3} M $(\text{NH}_4)_2\text{Fe}(\text{SO}_4)_2$. [TPE-2E N-oxide] = 2×10^{-3} M. B) The size distribution of TPE-2E N-oxide (2×10^{-3} M) dispersed in DI water with or without adding 20×10^{-3} M of $(\text{NH}_4)_2\text{Fe}(\text{SO}_4)_2$. C) The photos of the aqueous solution of 2×10^{-3} M of TPE-2E N-oxide before (left) and after (right) treated with 20×10^{-3} M of $(\text{NH}_4)_2\text{Fe}(\text{SO}_4)_2$ taken under UV light.

Glutathione (GSH) is one of the important antioxidants existing in the cellular environment, it failed to reduce the N-oxides as well (Figure S18C, Supporting Information). As the present N-oxides show no strong physical and chemical interactions with proteins and GSH, they are thus potential contrasting agents for turn-on bioimaging with good selectivity.

2.4. Hypoxia Imaging In Vitro

Driven by the intriguing properties of the present molecules, we then evaluated whether those probes were capable of detecting hypoxia in living cells. The HeLa cells were incubated with N-oxides for 3 h at various oxygen concentrations. As shown in Figure 5, strong fluorescence was observed in TPE-2M N-oxide and TPE-2M2F N-oxide when they were incubated with HeLa cells under both normoxic and hypoxic conditions. In contrast, TPE-2E N-oxide afforded a dark background under normoxia due to its AIE effect and zwitterionic character. Under hypoxic condition, it exhibited an oxygen-dependent light-up behavior. Especially, our probe could response to oxygen concentration at a concentration of 8%, which was truly impressive. It was reported that N-oxides in living systems predominantly underwent reduction by CYP450 reductase.^[21] Microsomes are heterogeneous vesicle-like artifacts with a diameter of 20–200 nm originated from the endoplasmic reticulum (ER) via the physical grinding of eukaryotic cells. They are considered

as a miscellaneous reductase system containing cytochrome P450 for evaluation of hypoxia imaging in vitro. As TPE-2E N-oxide had the best performance for hypoxia detection, it was incubated with rat liver microsomes and nicotinamide adenine dinucleotide phosphate as a cofactor under hypoxia and normoxia (Figure S19A, Supporting Information). Under the normoxic environment, PL was slightly enhanced by 2.44-fold. However, much higher PL enhancement was observed when the measurement was carried out under hypoxia condition. These results indicated that TPE-2E N-oxide could be rapidly reduced to its amine counterpart by CYP450 reductase encapsulated in the microsomes. The fluorescence responses of the TPE-2M N-oxide and TPE-2M2F N-oxide toward reductases in vitro were also investigated. As shown in Figure S19B,C (Supporting Information), both of TPE-2M N-oxide and TPE-2M2F N-oxide failed to be reduced by microsomes and no enhanced emission was found, suggesting that other intracellular enzymes might involve in the reduction of these two N-oxides.

Inhibition assay was performed using diphenyliodonium chloride (DPI) as an inhibitor of CYP450 reductase.^[21] The fluorescent microscopic images provided in Figure 6 and Figure S20 (Supporting Information) clearly showed that the reduction of TPE-2E N-oxide was progressively suppressed with increasing DPI concentration. Results from flow cytometry analysis shown in Figure 6 were also in good agreement with those of confocal images. As demonstrated in Figure S21 (Supporting Information), DPI did not inhibit the accumulation of TPE-2E

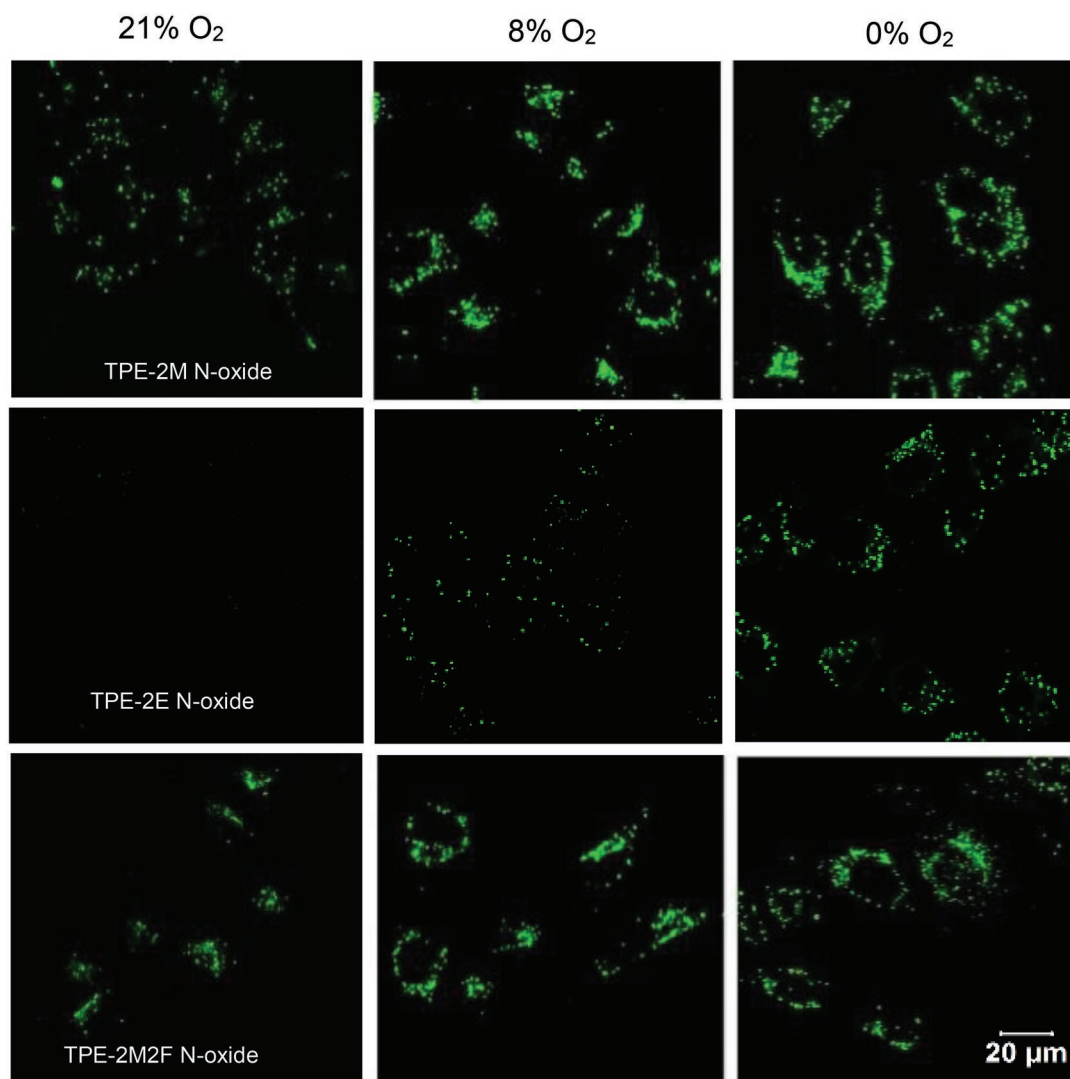


Figure 5. Fluorescent images of HeLa cells cultured with TPE-2M N-oxide, TPE-2E N-oxide, and TPE-2M2F N-oxide (200×10^{-6} M). The HeLa cells were incubated at various oxygen concentrations for 3 h.

in HeLa cells. It was posited that the reduction of TPE-2E N-oxide could be mediated by CYP450 reductase. However, the HeLa cells treated with TPE-2M N-oxide and TPE-2M2F N-oxide still fluoresced under hypoxic and normoxic conditions, even at high DPI concentrations (Figures S22 and S23, Supporting Information). Hence, we supposed that other enzymes, including xanthine oxidase and aldehyde oxidase, also took part in the metabolism of the N-oxides.^[22] With regard to the low sensitivity of TPE-2M N-oxide and TPE-2M2F N-oxide to oxygen deficiency, one possible explanation was that their molecular structures perfectly matched with the binding pocket of the involved enzyme. Thus, they preferred to interact with enzyme rather than oxygen to lead to their strong fluorescence under normoxic condition. On the other hand, the structure of TPE-2E N-oxide was not optimal to CYP450 reductase. Akin to an inhibitor of CYP450 reductase, oxygen could competitively occupy the active site of the enzyme. Therefore, TPE-2E N-oxide showed no response under normoxia condition. In the oxygen-free environment, TPE-2E N-oxide acted as the only “candidate”

to bind to the heme moiety of CYP450 reductase, whose reduction generated emissive TPE-2E. The higher the concentration of TPE-2E N-oxide used for bioimaging was, the stronger the PL intensity became (Figure S24, Supporting Information). This could be the reason why TPE-2E N-oxide was able to detect different oxygen deficiencies in tumor cells.

2.5. Lipid Droplet-Selective Staining and 3-(4,5-Dimethylthiazol-2-yl)-2,5-Diphenyltetrazolium Bromide (MTT) Assay

Figure 7 depicted the confocal images of HeLa cells co-stained with TPE-2E N-oxide and Nile red under hypoxia condition. The reduced form of TPE-2E N-oxide mainly located in the lipid droplets. The correlation coefficient of the two images was calculated to be 86%. To the best of our knowledge, TPE-2E N-oxide is the first hypoxia imaging probe capable of staining lipid droplets yet with a simple chemical structure. Meanwhile, such a strategy of releasing the precipitating fluorochrome is also

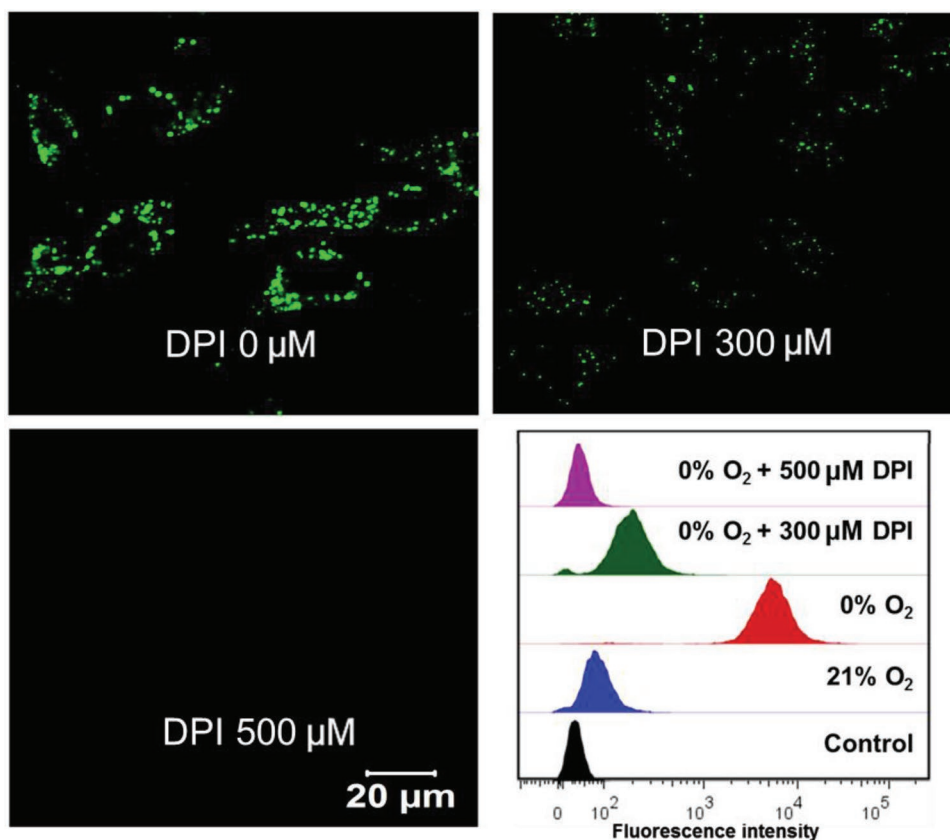


Figure 6. Fluorescent images of HeLa cells incubated with TPE-2E N-oxide (200×10^{-6} M) and different DPI concentrations for 3 h under hypoxic condition. Results from flow cytometry analysis of HeLa cells incubated with TPE-2E N-oxide were also shown here.

conductive to achieve long-term imaging benefiting from its diffusion-resistant feature.^[23] Compared with TPE-2M N-oxide and TPE-2M2F N-oxide, TPE-2E N-oxide exhibited better biocompatibility to HeLa cells and COS-7 cells through MTT assay due to its modest metabolic rate (Figures S25 and S26, Supporting Information). It was inferred that the rapid metabolism of TPE-2M N-oxide and TPE-2M2F N-oxide was prone to alter the subcellular redox equilibrium, which caused the cell death. Notably, the cytotoxicity of TPE-2M N-oxide to HeLa cells in hypoxic condition was higher than in normoxic condition, indicating that TPE-2M N-oxide could selectively kill cancer cells at low oxygen concentration and potentially serve as an AIE-active theranostic system.

3. Conclusion

In conclusion, we developed an exquisite tactic for designing water-soluble AIEgens for hypoxia imaging. The synthesis of TPE-2M N-oxide, TPE-2E N-oxide, and TPE-2M2F N-oxide was simple. The marriage of AIE-active TPE group and zwitterionic N-oxide functionality imparted these N-oxides with non-emissive character in the molecularly dispersed state. Upon addition of Fe^{2+} , the N-oxides showed different fluorescence response owing to the different substituent groups. Through bioimaging study, we found that TPE-2E N-oxide exhibited an

oxygen-dependent light-up behavior in HeLa cells with excellent biocompatibility. The metabolite of TPE-2E N-oxide selectively accumulated in the lipid droplets. Because of the outstanding properties of the TPE-based N-oxides, this work presented a new path to theranostic systems based on AIEgens.

4. Experimental Section

Materials and Instruments: All the reagents and solvents were purchased from AIEgen Biotech, J&K Chemicals, and Sigma-Aldrich. They were used as received without further purification. Microsomes were bought from Wuhan PrimeTox Bio-medical Technology Co. Ltd. ^1H and ^{13}C NMR spectra were measured on a Bruker AVII 400 NMR spectrometer using tetramethylsilane (TMS) as internal reference. High-resolution mass spectra (HRMS) were acquired on a GCT Premier CAB 048 mass spectrometer operated in matrix-assisted laser desorption ionization time-of-flight (MALDI-TOF) mode. Single-crystal data were collected on a Bruker Smart APEXII charge-coupled device (CCD) diffractometer using graphite monochromated $\text{Cu K}\alpha$ radiation ($\lambda = 1.54178$ Å). Absorption spectra were taken on a Milton Roy Spectronic 3000 Array spectrophotometer. PL spectra were measured on a Perkin-Elmer spectrofluorometer LS 55. Fluorescence quantum yields were measured using a Hamamatsu absolute PL quantum yield spectrometer C11347 Quantaaurus_QY. The nanoparticle morphology was observed using a transmission electron microscopy (TEM, JEM-2010F, 3JEOL, Japan). Particle-size analysis was determined at room temperature using a Zetaplus potential analyzer (Brookhaven Instruments Corporation). Laser confocal scanning microscopic images were collected on Zeiss

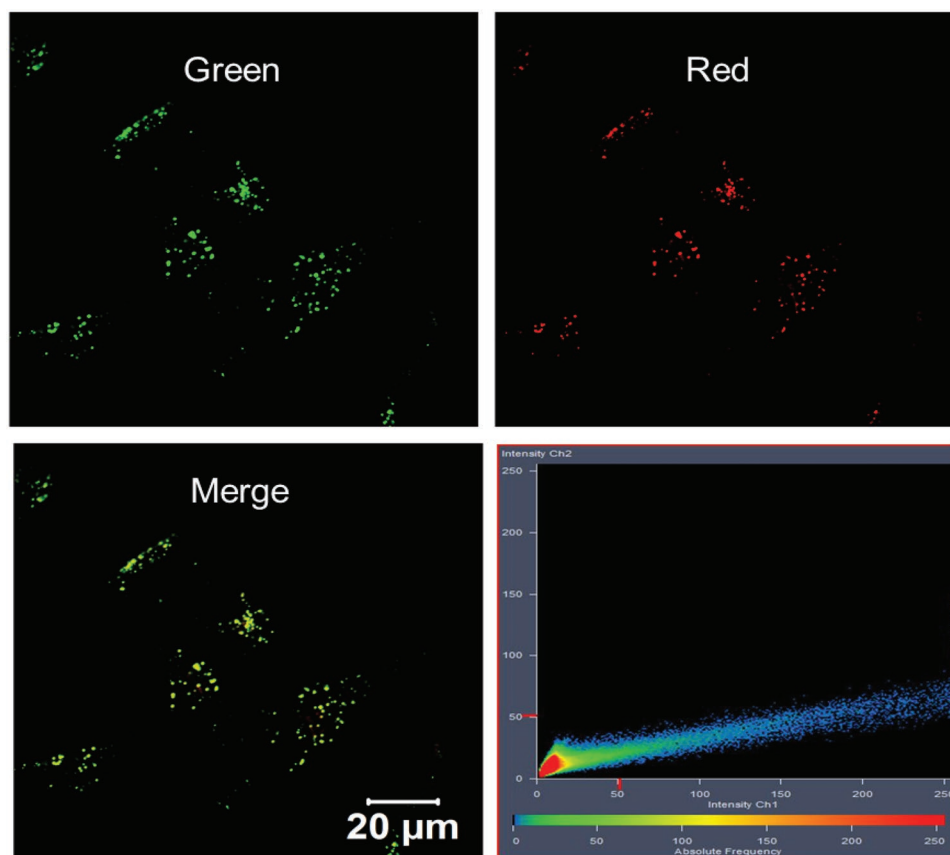


Figure 7. Confocal images of HeLa cells co-stained with TPE-2E N-oxide (200×10^{-6} M, green, 3 h) and Nile red (100 ng mL^{-1} , red, 15 min) under hypoxic condition. The excitation and emission wavelengths were 405 and 430–560 nm for TPE-2M N-oxide, TPE-2E N-oxide, and TPE-2M2F N-oxide, and 560 and 580–700 nm for Nile red, respectively.

laser scanning confocal microscope (LSM7 DUO) and analyzed using ZEN 2009 software (Carl Zeiss). The fluorescence intensity from flow cytometry was obtained from Becton Dickinson FACS Aria IIIu.

Synthesis of TPE-2M: To a 250 mL two-necked round-bottom flask equipped with a reflux condenser, 3.22 g (12 mmol) of 4,4'-bis(dimethylamino)benzophenone, 2.00 g (11 mmol) of benzophenone, and 4.18 g (64 mmol) of zinc dust were added. The whole reaction system was pumped by vacuum and purged with dry nitrogen for three times. Then freshly distilled fresh THF (80 mL) was injected into the flask with stirring for 15 min until all the reactants except zinc dust dissolved in THF completely. Subsequently, the flask was immersed into dry ice acetone bath (-80°C) and 3.53 mL of TiCl_4 was added dropwise into the flask with a syringe. After the mixture was stirred for 30 min, the reaction mixture was warmed up to room temperature and stirring was continued under refluxing for overnight. The final mixture was quenched with saturated sodium bicarbonate solution and extracted with dichloromethane for three times. The combined filtrate was dried with anhydrous sodium sulfate. After solvent evaporation, the crude product was purified with a silica gel chromatographic column using dichloromethane/hexane mixture (2:1, v/v) as the eluent. A luminous yellow product was obtained in 40% yield. $^1\text{H NMR}$ (CDCl_3 , 400 MHz), δ (TMS, ppm): 7.04–7.12 (m, 10H), 6.88–6.91 (d, 4H, $J = 8.8$ Hz), 6.44–6.46 (d, 4H, $J = 8.8$ Hz), 2.89 (s, 12H). $^{13}\text{C NMR}$ (CDCl_3 , 100 MHz), δ (TMS, ppm): 148.8, 145.3, 141.2, 136.9, 132.6, 132.4, 131.6, 127.6, 125.5, 111.4, 40.4.

Synthesis of TPE-2M N-Oxide: 200 mg of TPE-2M was dissolved in 10 mL of ethyl acetate and the reaction mixture was then placed at ice bath. After 190 mg of meta-chloroperoxybenzoic acid (*m*-CPBA) was added, the obtained mixture was stirred for 2 h. The crude product was

concentrated and purified with a silica gel chromatographic column using methanol as the eluent. The combined eluent was evaporated and the product was redissolved in dichloromethane. The mixture was filtered to remove the silica gel. The dichloromethane solution was condensed to afford a white powder in 80% yield. $^1\text{H NMR}$ (CDCl_3 , 400 MHz), δ (TMS, ppm): 7.66–7.68 (d, 4H, $J = 8.8$ Hz), 7.08–7.12 (m, 10H), 6.90–7.01 (m, 4H), 3.52 (s, 12H). $^{13}\text{C NMR}$ (CD_3OD , 100 MHz), δ (TMS, ppm): 151.9, 144.4, 144.1, 142.6, 137.6, 131.8, 130.8, 127.7, 126.9, 119.3, 61.5. HRMS (MALDI-TOF), m/z calcd. for $\text{C}_{30}\text{H}_{30}\text{N}_2\text{O}_2$: 450.2307; found 418.2447 [$\text{C}_{30}\text{H}_{30}\text{N}_2$] $^+$.

Synthesis of TPE-2E: TPE-2E was synthesized by following a procedure similar to TPE-2M. Yield: 35%. $^1\text{H NMR}$ (CDCl_3 , 400 MHz), δ (TMS, ppm): 7.05–7.12 (m, 10H), 6.88–6.90 (d, 4H, $J = 8.8$ Hz), 6.41–6.43 (d, 4H, $J = 8.8$ Hz), 3.27–3.33 (q, 8H), 1.11–1.15 (t, 12H, $J = 7.2$ Hz). $^{13}\text{C NMR}$ (CDCl_3 , 100 MHz), δ (TMS, ppm): 146.3, 145.6, 141.5, 136.1, 132.8, 131.6, 131.3, 127.5, 125.3, 110.8, 44.2, 12.7.

Synthesis of TPE-2E N-Oxide: TPE-2E N-oxide was synthesized by following a procedure similar to TPE-2M N-oxide. Yield: 75%. $^1\text{H NMR}$ (CDCl_3 , 400 MHz), δ (TMS, ppm): 7.52–7.54 (d, 4H, $J = 8.4$ Hz), 7.06–6.97 (m, 10H), 6.93–6.97 (d, 4H, $J = 7.6$ Hz), 3.56–3.61 (m, 8H), 1.08–1.12 (t, 12H, $J = 6.8$ Hz). $^{13}\text{C NMR}$ (CD_3OD , 100 MHz), δ (TMS, ppm): 146.6, 143.9, 143.8, 142.7, 138.3, 131.6, 131.0, 127.7, 127.0, 121.5, 66.4, 7.4. HRMS (MALDI-TOF), m/z calcd. for $\text{C}_{34}\text{H}_{38}\text{N}_2\text{O}_2$: 506.6900; found 474.3019 [$\text{C}_{34}\text{H}_{38}\text{N}_2$] $^+$.

Synthesis of TPE-2M2F: Yield: 38%. $^1\text{H NMR}$ (CDCl_3 , 400 MHz), δ (TMS, ppm): 6.98–7.03 (m, 4H), 6.86–6.93 (d, 4H, $J = 8.8$ Hz), 6.77–6.85 (m, 4H), 6.45–6.51 (d, 4H, $J = 8.8$ Hz), 2.90 (s, 12H). $^{13}\text{C NMR}$ (CDCl_3 , 100 MHz), δ (TMS, ppm): 162.2, 159.7, 148.9, 141.7, 141.0, 141.0, 134.5, 133.0, 132.9, 132.5, 131.9, 114.7, 114.5, 111.4, 40.4.

Synthesis of TPE-2M2F N-Oxide: Yield: 85%. ¹H NMR (CDCl₃, 400 MHz), δ (TMS, ppm): 7.71–7.73 (d, 4H, J = 8.8 Hz), 7.06–7.12 (d, 4H, J = 8.8 Hz), 6.92–7.00 (m, 4H), 6.78–6.86 (m, 4H), 3.56 (s, 12H). ¹³C NMR (CD₃OD, 100 MHz), δ (TMS, ppm): 163.1, 160.7, 152.0, 144.1, 141.8, 138.6, 138.6, 138.3, 132.7, 132.6, 131.8, 119.5, 114.7, 114.5, 61.6. HRMS (MALDI-TOF), m/z calcd. for C₃₀H₂₈F₂N₂O₂: 486.2119; found 454.2207 [C₃₀H₂₈F₂N₂]⁺.

Cell Culture: HeLa cells were cultured in minimum Eagle's medium (MEM) containing 10% fetal bovine serum (Invitrogen) and 100 units mL⁻¹ penicillin and 100 mg mL⁻¹ streptomycin. COS-7 cells were cultured in Dulbecco's modified Eagle medium supplemented with 10% fetal bovine serum (Invitrogen) and 100 units mL⁻¹ penicillin and 100 mg mL⁻¹ streptomycin. The cells were incubated in a standard incubator, maintained at 37 °C under 5% CO₂ and 21% O₂, providing a normoxic condition. Hypoxic incubator was performed by incubating the cells in a 2.5 L rectangular sealed container with Anaero Pack-Anaero anaerobic gas generator (0.1% O₂ concentration) or AnaeroPack-MicroAero gas generator (8% O₂ concentration). Hypoxic conditions were confirmed by the use of MGC RT Anaero-Indicator.

Cell Imaging: Cells were cultured overnight in a 35 mm Petri dish with coverslip. The cell medium was replaced with fresh one and the cells were stained with 100 μg mL⁻¹ of TPE-2M N-oxide, TPE-2E N-oxide, or TPE-2M2F N-oxide for 3 h under different oxygen conditions. Subsequently, the cell coverslip was taken out and the dish was mounted. The cells were imaged using a laser scanning confocal microscope (LSM710, Zeiss) at 405 nm with 2% laser power. The emission filter was 430–560 nm.

Flow Cytometry: Cells were seeded and treated with TPE-2E N-oxide under different oxygen conditions for 3 h. The fluorescence was measured using a Becton–Dickinson flow cytometer Aria IIIu with an excitation wavelength of 405 nm. 10 000 cells were counted. The data were analyzed using Flowjo.

Cytotoxicity Study: Cell viability was evaluated by MTT assay. Cells were seeded in 96-well plates overnight at a density of 5000–8000 cells per well. Then the medium was replaced with 200 μL fresh MEM medium containing various concentrations of TPE-2M N-oxide, TPE-2E N-oxide, or TPE-2M2F N-oxide, and the cells were incubated under normoxic or hypoxic conditions. After 24 h, 10% MTT solution was added into the medium, followed by adding 100 μL dimethyl sulfoxide. The plates were analyzed with a microplate reader (Varioskan LUX multimode microplate reader) with the absorbance at 595 nm. Each experiment was performed at least three times.

Inhibitor Assay: A certain amount of DPI was dissolved in Milli-Q water to serve as a stock solution. The cells were incubated with TPE-2M N-oxide, TPE-2E N-oxide, or TPE-2M2F N-oxide in the presence of various concentrations of DPI (0, 300 × 10⁻⁶, and 500 × 10⁻⁶ M) under different oxygen conditions for 3 h.

Confocal Colocalization: HeLa cells were incubated under hypoxic condition with TPE-2E N-oxide for 3 h. The medium was removed and washed with phosphate buffered saline buffer solution. Then Nile red (100 ng mL⁻¹) was added for 15 min. Imaging of the HeLa cells was conducted under a confocal microscope. The excitation wavelength of the reduced form of TPE-2E N-oxide was 405 nm, and the emission filter was 430–560 nm. For Nile red, the excitation was 560 nm and the emission filter was 580–700 nm.

Supporting Information

Supporting Information is available from the Wiley Online Library or from the author.

Acknowledgements

C.X. and H.Z. contributed equally to this work. This work was partially supported by the National Natural Science Foundation of China (Grant No. 21788102), the University Grants Committee of Hong Kong (AoE/P-03/08), the Research Grants Council of Hong Kong (16305015,

A-HKUST 605/16, C6009-17G, and N_HKUST604/14), the Innovation and Technology Commission (ITC-CNERC14SC01, ITCPD/17-9, and ITCPD/17-9), and the Science and Technology Plan of Shenzhen (JCYJ20170818113602462 and JCYJ20160229205601482).

Conflict of Interest

The authors declare no conflict of interest.

Keywords

aggregation-induced emission, hypoxia, N-oxide, sensitivity, water solubility

Received: April 24, 2019

Revised: May 30, 2019

Published online:

- [1] J. Bernier, *Head and Neck Cancer: Multimodality Management*, Springer Science & Business Media, Berlin 2011.
- [2] P. Vaupel, L. Harrison, *Oncologist* 2004, 9, 4.
- [3] Y. Cao, C.-Y. Li, B. J. Moeller, D. Yu, Y. Zhao, M. R. Dreher, S. Shan, M. W. Dewhirst, *Cancer Res.* 2005, 65, 5498.
- [4] a) M. Zhang, Z. Zhou, Z. Zhao, J. Garrison, *Explor. Res. Hypothesis Med.* 2016, 1, 17; b) W.-J. Koh, K. S. Bergman, J. S. Rasey, L. M. Peterson, M. L. Evans, M. M. Graham, J. R. Grierson, K. L. Lindsley, T. K. Lewellen, K. A. Krohn, *Int. J. Radiat. Oncol., Biol., Phys.* 1995, 33, 391.
- [5] M. W. Gross, U. Karbach, K. Groebe, A. J. Franko, W. Mueller-Klieser, *Int. J. Cancer* 1995, 61, 567.
- [6] a) W. Piao, S. Tsuda, Y. Tanaka, S. Maeda, F. Liu, S. Takahashi, Y. Kushida, T. Komatsu, T. Ueno, T. Terai, *Angew. Chem., Int. Ed.* 2013, 52, 13028; b) H. Komatsu, H. Harada, K. Tanabe, M. Hiraoka, S.-i. Nishimoto, *MedChemComm* 2010, 1, 50; c) S. Luo, R. Zou, J. Wu, M. P. Landry, *ACS Sens.* 2017, 2, 1139; d) P. Zhang, H. Huang, Y. Chen, J. Wang, L. Ji, H. Chao, *Biomaterials* 2015, 53, 522.
- [7] a) K. Kiyose, K. Hanaoka, D. Oushiki, T. Nakamura, M. Kajimura, M. Suematsu, H. Nishimatsu, T. Yamane, T. Terai, Y. Hirata, *J. Am. Chem. Soc.* 2010, 132, 15846; b) S. Luo, Y. Liu, F. Wang, Q. Fei, B. Shi, J. An, C. Zhao, C.-H. Tung, *Analyst* 2016, 141, 2879; c) L. Cui, Y. Shi, S. Zhang, L. Yan, H. Zhang, Z. Tian, Y. Gu, T. Guo, J. Huang, *Dyes Pigm.* 2017, 139, 587; d) L. Sun, G. Li, X. Chen, Y. Chen, C. Jin, L. Ji, H. Chao, *Sci. Rep.* 2015, 5, 14837.
- [8] a) J. Luo, Z. Xie, J. W. Lam, L. Cheng, H. Chen, C. Qiu, H. S. Kwok, X. Zhan, Y. Liu, D. Zhu, B. Z. Tang, *Chem. Commun.* 2001, 1740; b) Y. Hong, J. W. Lam, B. Z. Tang, *Chem. Soc. Rev.* 2011, 40, 5361; c) J. Mei, N. L. Leung, R. T. Kwok, J. W. Lam, B. Z. Tang, *Chem. Rev.* 2015, 115, 11718; d) J.-S. Ni, H. Liu, J. Liu, M. Jiang, Z. Zhao, Y. Chen, R. T. Kwok, J. W. Y. Lam, Q. Peng, B. Z. Tang, *Mater. Chem. Front.* 2018, 2, 1498; e) Y. Zhang, W. Xu, L. Kong, B. Han, Z. Cai, J. Shi, B. Tong, Y. Dong, B. Z. Tang, *Mater. Chem. Front.* 2018, 2, 1779; f) V. G. Naik, S. D. Hiremath, A. Das, D. Banwari, R. U. Gawas, M. Biswas, M. Banerjee, A. Chatterjee, *Mater. Chem. Front.* 2018, 2, 2091.
- [9] a) N. L. Leung, N. Xie, W. Yuan, Y. Liu, Q. Wu, Q. Peng, Q. Miao, J. W. Lam, B. Z. Tang, *Chem. - Eur. J.* 2014, 20, 15349; b) F. Bu, R. Duan, Y. Xie, Y. Yi, Q. Peng, R. Hu, A. Qin, Z. Zhao, B. Z. Tang, *Angew. Chem., Int. Ed.* 2015, 54, 14492.

- [10] a) D. Ding, K. Li, B. Liu, B. Z. Tang, *Acc. Chem. Res.* **2013**, *46*, 2441; b) X. Wang, J. Hu, G. Zhang, S. Liu, *J. Am. Chem. Soc.* **2014**, *136*, 9890; c) H. Shi, R. T. Kwok, J. Liu, B. Xing, B. Z. Tang, B. Liu, *J. Am. Chem. Soc.* **2012**, *134*, 17972.
- [11] S. Xie, A. Y. Wong, R. T. Kwok, Y. Li, H. Su, J. W. Lam, S. Chen, B. Z. Tang, *Angew. Chem., Int. Ed.* **2018**, *57*, 5750.
- [12] O. Trédan, A. B. Garbens, A. S. Lalani, I. F. Tannock, *Cancer Res.* **2009**, *69*, 940.
- [13] M. F. Belcourt, W. F. Hodnick, S. Rockwell, A. C. Sartorelli, *Proc. Natl. Acad. Sci. USA* **1996**, *93*, 456.
- [14] a) R. Hu, E. Lager, A. Aguilar-Aguilar, J. Liu, J. W. Lam, H. H. Sung, I. D. Williams, Y. Zhong, K. S. Wong, E. Pena-Cabrera, B. Z. Tang, *J. Phys. Chem. C* **2009**, *113*, 15845; b) Y. Zhang, D. Li, Y. Li, J. Yu, *Chem. Sci.* **2014**, *5*, 2710.
- [15] a) V. S. Padalkar, D. Sakamaki, K. Kuwada, N. Tohnai, T. Akutagawa, K.-i. Sakai, S. Seki, *RSC Adv.* **2016**, *6*, 26941; b) M. Yang, D. Xu, W. Xi, L. Wang, J. Zheng, J. Huang, J. Zhang, H. Zhou, J. Wu, Y. Tian, *J. Org. Chem.* **2013**, *78*, 10344.
- [16] a) S. A. Fateminia, Z. Wang, C. C. Goh, P. N. Manghnani, W. Wu, D. Mao, L. G. Ng, Z. Zhao, B. Z. Tang, B. Liu, *Adv. Mater.* **2017**, *29*, 1604100; b) Y. Lin, G. Chen, L. Zhao, W. Z. Yuan, Y. Zhang, B. Z. Tang, *J. Mater. Chem. C* **2015**, *3*, 112; c) Y. Dong, J. W. Lam, A. Qin, Z. Li, J. Sun, H. H.-Y. Sung, I. D. Williams, B. Z. Tang, *Chem. Commun.* **2007**, 40.
- [17] L. H. Patterson, *Cancer Metastasis Rev.* **1993**, *12*, 119.
- [18] a) T. Hirayama, H. Tsuboi, M. Niwa, A. Miki, S. Kadota, Y. Ikeshita, K. Okuda, H. Nagasawa, *Chem. Sci.* **2017**, *8*, 4858; b) T. Hirayama, K. Okuda, H. Nagasawa, *Chem. Sci.* **2013**, *4*, 1250.
- [19] a) X. He, Z. Zhao, L.-H. Xiong, P. F. Gao, C. Peng, R. S. Li, Y. Xiong, Z. Li, H. H.-Y. Sung, I. D. Williams, B. Z. Tang, *J. Am. Chem. Soc.* **2018**, *140*, 6904; b) G. P. Maier, C. M. Bernt, A. Butler, *Biomater. Sci.* **2018**, *6*, 332; c) G. Canard, M. Ponce-Vargas, D. Jacquemin, B. Le Guennic, A. Felouat, M. Rivoal, E. Zaborova, A. D'Aléo, F. Fages, *RSC Adv.* **2017**, *7*, 10132.
- [20] L. Zhang, J. Du, *Spectrochim. Acta, Part A* **2016**, *158*, 24.
- [21] H. J. Knox, J. Hedhli, T. W. Kim, K. Khalili, L. W. Dobrucki, J. Chan, *Nat. Commun.* **2017**, *8*, 1794.
- [22] a) K. Takekawa, S. Kitamura, K. Sugihara, S. Ohta, *Xenobiotica* **2001**, *31*, 11; b) K. N. Murray, S. Chaykin, *J. Biol. Chem.* **1966**, *241*, 3468.
- [23] a) H. W. Liu, K. Li, X. X. Hu, L. Zhu, Q. Rong, Y. Liu, X. B. Zhang, J. Hasserodt, F. L. Qu, W. Tan, *Angew. Chem.* **2017**, *129*, 11950; b) K. Li, X.-X. Hu, H.-W. Liu, S. Xu, S. Huan, J.-B. Li, T.-G. Deng, X.-B. Zhang, *Anal. Chem.* **2018**, *90*, 11680.